1994

Thermal Characteristics of a Nickel-Hydrogen Battery

Junbom Kim
University of South Carolina - Columbia

T. V. Nguyen
University of South Carolina - Columbia

Ralph E. White
University of South Carolina - Columbia, white@cec.sc.edu

Publication Info

Journal of the Electrochemical Society, 1994, pages 333-338.

Publisher's link: http://dx.doi.org/10.1149/1.2054726
DOI: 10.1149/1.2054726

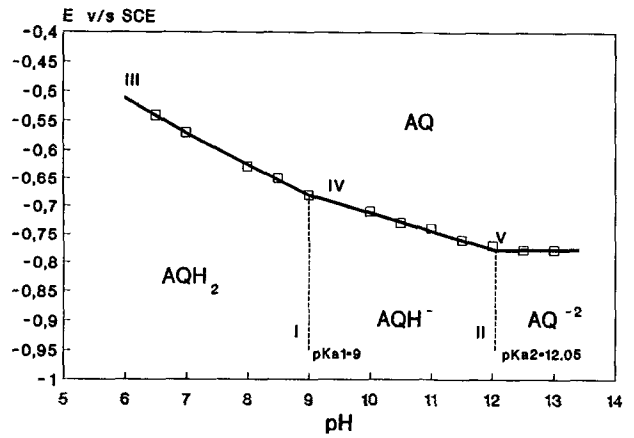

Fig. 2. *E*-pH graph of anthraquinone on H_2O-5% DMF at 25°C between pH 6 and 14. Characteristic parameters: $pK_{a1} = 9$; $pK_{a2} = 12.05$; $E^\circ_{AQ/AQ^{-2}} = -0.778$ V. Line III ($r^2 = 0.995$, slope = -0.057 V · pH^{-1}), Line IV ($r^2 = 0.991$, slope = -0.028 V · pH^{-1}).

AQH_2	9,10-dihydroxyanthracene
DMF	N,N-dimethyl formamide
$E_{1/2}$	half-wave potential
K_D	disproportionation constant
K_S	stability constant of anthrasemiquinone
K_{a1}	first ionization constant of AQH_2
K_{a2}	second ionization constant of AQH_2
n	charge number of cell reaction
pK_i	$pK_{ai} = -\log K_{ai}$
T	temperature (K)

REFERENCES

1. D. Meisel and R. Fesseden, *J. Am. Chem. Soc.*, **98,** 7505 (1976).
2. T. Nagaokan and S. Okazaki, *J. Phys. Chem.*, **89,** 2340 (1985).
3. S. Howell and R. Wightman, *Anal. Chem.*, **56,** 524 (1984).
4. W. Bowyer, E. Engelman, and D. Evans, *J. Electroanal. Chem.*, **262,** 67 (1989).
5. M. Pournaghi-Azar and S. Golabi, *Talanta,* **35,** 959 (1988).
6. D. Wipf, K. Wehmeyer, and R. Wightman, *J. Org. Chem.*, **51,** 4761 (1986).
7. P. He, R. Crooks, and L. Faulkner, *J. Phys. Chem.*, **94,** 1134 (1990).
8. R. Gill and H. Stonehill, *J. Chem. Soc.*, 1845 (1952).
9. C. Qureshi, G. Svehla, and M. Leonard, *Analyst,* **104,** 704 (1979).
10. F. Rodríguez, J. Revenga, C. Negro, and J. Tijero, *Inv. Tec. Papel.*, **30,** 74 (1993).
11. P. Given and M. Peover, *J. Chem. Soc.*, 394 (1960).
12. A. Aumüller and S. Hünig, *Liebigs Ann. Chem.*, **101,** 165 (1988).
13. J. Heyrovsky, *Principles of Polarography,* Chap. 9, 11 Academic Press, New York (1966).
14. D. Tanner and N. Deonarian, *Can. J. Chem.*, **67,** 171 (1989).

Thermal Characteristics of a Nickel-Hydrogen Battery

Junbom Kim,*[a] T. V. Nguyen,*[b] and R. E. White*

Department of Chemical Engineering, University of South Carolina, Columbia, South Carolina 29208

ABSTRACT

The maximum allowable temperature difference inside a nickel-hydrogen battery to avoid water relocation was calculated by using a graphical method together with a vapor pressure *vs.* temperature correlation equation for water vapor over potassium hydroxide solution. An equation was developed for this maximum allowable temperature difference for vessel-wall temperatures from 0 to 30°C and potassium hydroxide concentrations from 20 to 32%. A heat-generation equation for the nickel-hydrogen battery was used to investigate the effect of the location of heat generation on the maximum temperature in the cell and the temperature distribution in the cell.

Even though a nickel-hydrogen battery offers higher energy density, longer life, and more tolerance to overcharge and reversal than a nickel-cadmium battery for spacecraft applications,[1-4] the nickel-hydrogen battery has some limitations. The tolerance to overcharge of a nickel-hydrogen battery is limited by the heat-rejection capability and the ability to recombine oxygen without damaging the internal cell structure.[5] Expansion of the nickel electrode, electrolyte redistribution, and pressure vessel leaks may limit the life of a nickel-hydrogen battery.[4,6] Electrolyte redistribution and nickel-electrode expansion result in dry areas and dead zones within the cell. There are three kinds of mechanisms: displacement, entrainment, and evaporation/condensation, which may cause electrolyte loss from the nickel electrode. Electrolyte loss by displacement due to mechanical impact during launch is not appreciable and the battery usually recovers from this loss after a few cycles. Electrolyte loss by entrainment was small during oxygen production in the nickel electrode and not found during hydrogen production in the platinum electrode.[7] However, evaporation/condensation may cause a continuing electrolyte movement problem if a large temperature gradient exists inside a nickel-hydrogen battery. Thus, we must understand the temperature profile inside a nickel-hydrogen battery to predict the occurrence of evaporation/condensation.[8] An equation is presented below that can be used to predict the maximum allowable temperature difference in nickel-hydrogen battery to avoid the evaporation/condensation problem.

A heat-generation equation is used here to study the effects of heat-generation location on the temperature profile inside a nickel-hydrogen battery. Two cases, heat generation only on the nickel electrode and heat generation only on the platinum electrode (hypothetical case), are compared using a constant heat-generation rate at steady state. For nonsteady-state cases, time-dependent heat-generation rates are calculated using the current efficiency during charge and cell voltage data during charge and discharge.[9] We assume that oxygen recombination occurs on the platinum electrode to split the heat-generation rate between the nickel and platinum electrodes. The two cases, heat generation only on the nickel electrode and heat generation on the nickel and platinum electrodes are compared

* Electrochemical Society Active Member.

[a] Present address: Center for Electrochemical Systems and Hydrogen Research, Texas A&M University, College Station, Texas 77843.

[b] Present address: AT&T Bell Laboratories, Mesquite, Texas 75149.

using time-dependent heat-generation rates to predict the temperature difference in a nonsteady-state case.

Reaction Mechanism

The main reactions of the nickel-hydrogen battery are presented in Eq. 1-3. The half-cell reaction at the nickel electrode of a nickel-hydrogen cell is similar to that of a nickel-cadmium cell during normal operation. Nickel hydroxide is oxidized to nickel oxyhydroxide at the nickel electrode and hydrogen gas is formed from the water at the platinum electrode during charge.

Nickel electrode

$$Ni(OH)_2 + OH^- \rightleftharpoons NiOOH + H_2O + e^- \quad [1]$$

Platinum electrode

$$H_2O + e^- \rightleftharpoons \frac{1}{2} H_2 + OH^- \quad [2]$$

Net reaction

$$Ni(OH)_2 \rightleftharpoons NiOOH + \frac{1}{2} H_2 \quad [3]$$

During charge, a side reaction occurs at the electrodes as given by Eq. 4-6 below. The side reaction rate increases toward the end of charge and becomes the major reaction during overcharge as the charging current efficiency drops. The side reaction produces oxygen on the nickel electrode but the platinum electrode reaction is the same as the main reaction and generates hydrogen during charge. Thus, the net electrochemical reaction is the electrolysis of water to produce hydrogen and oxygen. The side reactions are presented in Eq. 4-6

Nickel electrode

$$2\ OH^- \rightarrow \frac{1}{2} O_2 + H_2O + 2e^- \quad [4]$$

Platinum electrode

$$2H_2O + 2e^- \rightarrow H_2 + 2\ OH^- \quad [5]$$

Net reaction

$$H_2O \rightarrow \frac{1}{2} O_2 + H_2 \quad [6]$$

We assume here that the oxygen produced on the nickel electrode during charge and overcharge is then recombined with hydrogen at the platinum electrode catalyst.[10] There is no net change in the potassium hydroxide concentration during the side reaction, but it produces heat which may cause a large temperature gradient and subsequent water movement.

Equation Formulation

An equation for temperature *vs.* vapor pressure of water and potassium hydroxide solution at various concentrations is needed to calculate the maximum allowable temperature difference in the nickel-hydrogen battery to avoid the water vapor evaporation/condensation problem. Bro and Kang[11] measured the vapor pressure of potassium hydroxide solution for the temperature range −40 to 25°C. Old tabulated data[12] is also available for the temperature range 0 to 100°C, and Mashovets and Matveeva[13] measured the vapor pressure up to 400°C. Anisimov provided a correlation of these two sets of data[12,13] and presented a table.[14] LeRoy and Bowen made a feasible correlation equation of the water vapor pressure over a potassium hydroxide solution, but temperature and solution concentration were not used simultaneously.[15] Balej[16] provides a correlation which overcomes this limitation as given by Eq. 7

$$\log P_{W(KOH)} = -0.01508M - 0.0016788M^2 + 2.25887 \times 10^{-5}M^3 + (1 - 0.0012062M + 5.6024 \times 10^{-4}M^2 - 7.8228 \times 10^{-6}M^3) \times \left(35.4462 - \frac{3343.93}{T^\star} - 10.9 \log T^\star + 0.0041645T^\star\right) \quad [7]$$

where $P_{W(KOH)}$, M, $T^\star$ are the vapor pressure, molality, and absolute temperature of the potassium hydroxide solution, respectively. This equation agrees well with the data[12,13] to within 3.8% in the ranges of 0 m to 18 m and 0 to 300°C.

Heat changes in the system can be expressed by Eq. 8 under the assumption of no kinetic and potential energy changes and a constant volume process

$$\frac{dQ}{dt} = \frac{\Delta H_a}{nF} \eta I + \frac{\Delta H_b}{nF} (1 - \eta) I - V \frac{dP}{dt} - EI - \dot{q}_o \quad [8]$$

where ΔH_a and ΔH_b are the enthalpy changes of Eq. 3 and 6 during charge and the values are 145.50 and 285.83 KJ · mol^{-1} respectively.[17-20] Other variables and constants are explained in the List of Symbols. The pressure prior to charge is assumed to be 50 psi and linearly increases to 600 psi at the end of charge and no change occurs during overcharge.[9] We assume here that the recombination rate of oxygen is the same as the production rate.[21] Thus, the two terms, heat change due to the production, $\Delta H_b/nF\,(1 - \eta)I$, and the heat generation due to oxygen recombination, $\dot{q}_o$, cancel each other. The heat-generation rate is equal to the heat change in the surroundings which is the minus value of the heat change in the system. Thus, heat-generation rate during charge can be expressed as follows

$$\dot{q} = -\frac{dQ}{dt} = I\left(E - \frac{\Delta H_a}{nF} \eta\right) + V \frac{dP}{dt} \quad [9]$$

where the calculated value of $\Delta H_a/nF$ is 1.508 V. It is assumed here that there are no side reactions during discharge. Thus, the heat-generation rate during discharge can be expressed as follows

$$\dot{q} = -\frac{dQ}{dt} = I\left(\frac{\Delta H_a}{nF} - E\right) + V \frac{dP}{dt} \quad [10]$$

Results and Discussion

One main cause limiting the life of the nickel-hydrogen battery is electrolyte loss from the cell stack. Water evaporation/condensation due to a temperature gradient inside the cell is the main cause of electrolyte loss from the cell stack. Since water vapor can travel inside the nickel-hydrogen battery freely, water vapor formation itself does not make electrolyte movement a problem as long as the vapor does not condense in other regions of the battery. Thus, the prediction of a maximum allowable temperature difference in the cell to avoid water vapor condensation in other regions should be helpful as a cell design guide to extend the nickel-hydrogen battery service life. Equation 7 is used to calculate water vapor pressure over potassium hydroxide solution in the ranges of 20 to 32 weight percent (w/o) and 0 to 45°C. The calculated vapor pressure values agree well with the experimentally measured data[12,13] to within 1.8% in these ranges.

Figure 1 presents these data and the vapor pressure for water. At 10°C the vapor pressure of water is 9.20 mm Hg and at 19.68°C the vapor pressure of the 32 w/o KOH solution is 9.20 mm Hg. When the coldest point inside a cell, usually the inner vessel wall, is 10°C, that position in the cell may contain water vapor up to 9.20 mm Hg. Thus, the allowable temperature difference in the cell to avoid water relocation is 9.68°C. Figure 2 presents plots of allowable temperature differences as a function of wall temperature for various concentrations of KOH. As can be seen in Fig. 2, the maximum allowable temperature difference at one concentration is almost linearly proportional to the wall temperature. Thus, the maximum allowable temperature difference is assumed here to be linearly proportional to the wall temperature, and can be expressed as

$$\Delta T = a + bT_c \quad [11]$$

where ΔT, T_c, a, and b are the maximum allowable temperature difference, the coldest point temperature in the nickel-hydrogen battery, intersecting point for T_c = 0°C

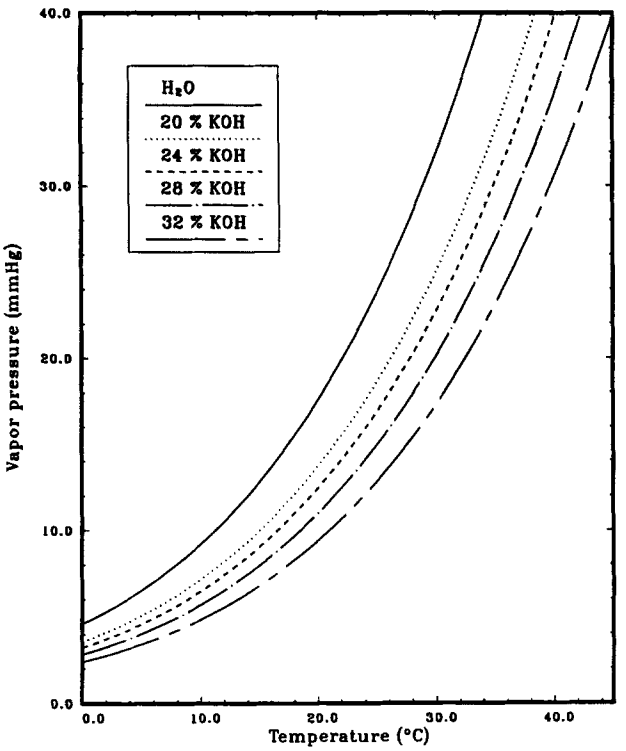

Fig. 1. Vapor pressure over potassium hydroxide solution.

and the slope of variable wall temperature at one potassium hydroxide concentration, respectively. Parameter values a and b are calculated for each potassium hydroxide concentration and are plotted in Fig. 3. Thus, by using Eq. 11 and a and b values from Fig. 3 one can predict the maximum allowable temperature difference in a cell. Correlations[22] between a and b values and potassium hydroxide concentration are as follows

$$a = 2.94872426 - 0.24737596W + 0.01376840\ W^2 \quad [12]$$

$$b = 0.01016541 - 0.00021840W + 5.04845 \times 10^{-5}W^2 \quad [13]$$

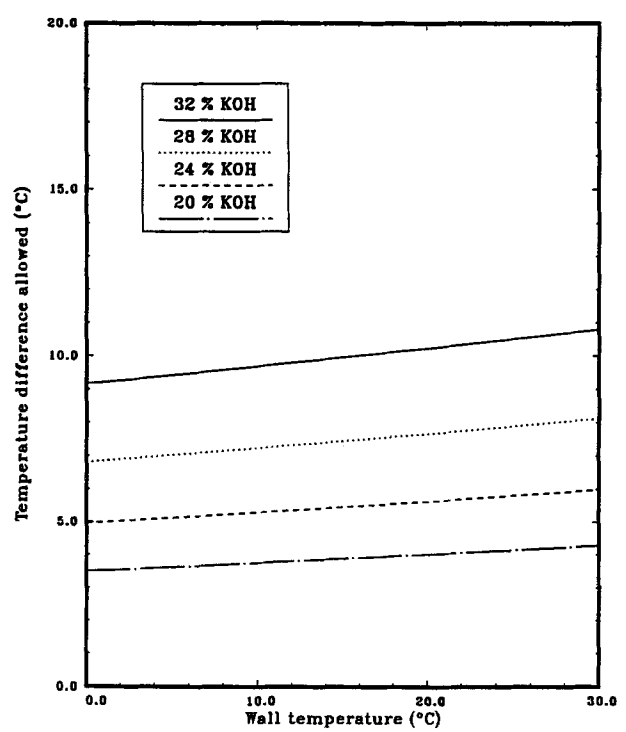

Fig. 2. The maximum allowable temperature difference in the nickel-hydrogen battery.

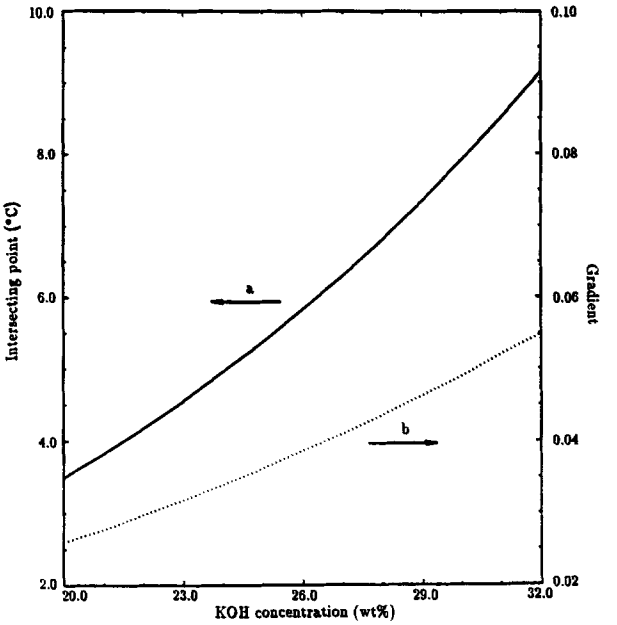

Fig. 3. Coefficients a and b in Eq. 11 *vs.* potassium hydroxide concentration plot.

where W represents the weight percent of potassium hydroxide solution. The resulting equation for calculating the maximum allowable temperature difference in this range is obtained by combining Eq. 11-13, and is expressed as Eq. 14

$$\Delta T = 2.94872426 - 0.24737596W + 0.01376840W^2$$
$$+ (0.01016541 - 0.00021840W + 5.04845 \times 10^{-5}W^2)T_c \quad [14]$$

The effect of the location of heat generation within a cell on the temperature profile within a cell was studied also. A schematic diagram of the cell studied here is shown in Fig. 4. There are two cells between heat fins, and one cell consists of three modules as shown in Fig. 4. By symmetry, only the dashed region is modeled to study the temperature profile of the region between heat fins. A detailed description of a module is given in the lower inset of Fig. 4, and

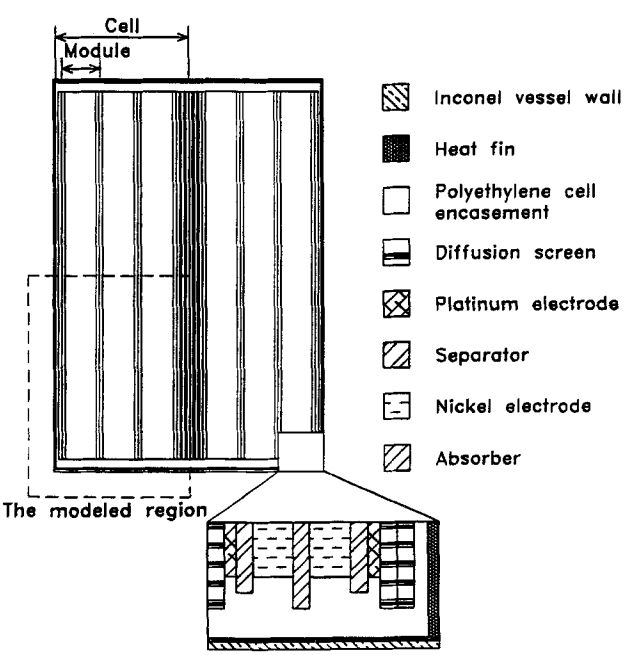

Fig. 4. Schematic representation of the nickel-hydrogen cell.

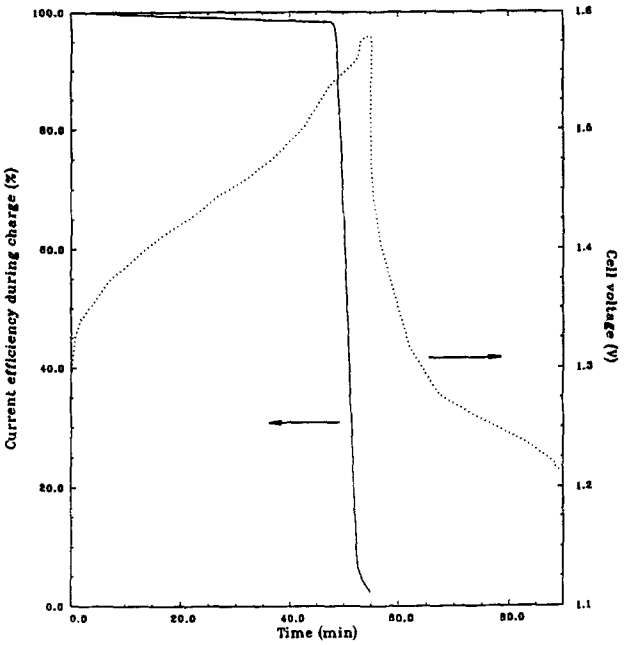

Fig. 5. Current efficiency during charge and the cell potential of a nickel-hydrogen battery from Johnson Controls, Inc. (55 min charge and 35 min, 40% depth of discharge for a low-earth-orbit regime).

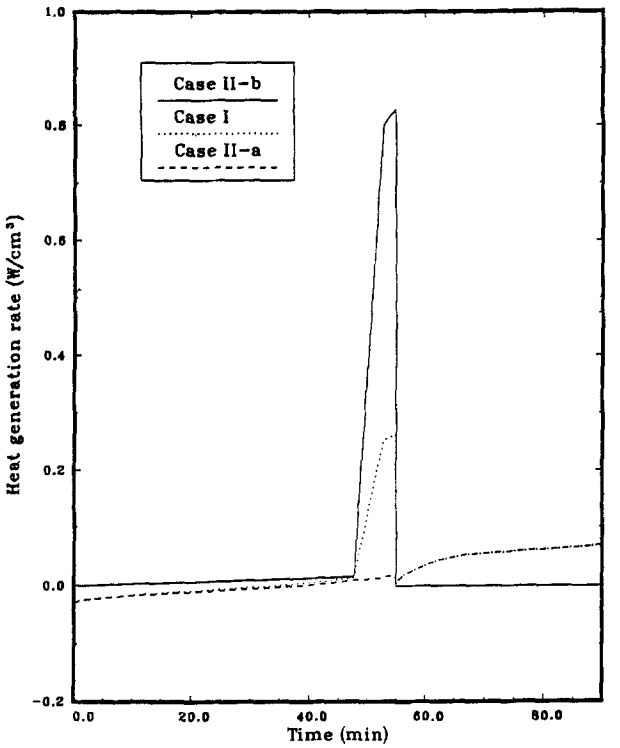

Fig. 6. Time-dependent heat-generation rate.

specification of the type of material in a module is shown on the right side of Fig. 4.

The current efficiency during charge and the cell potential during one cycle (55 min charge and 35 min, 40% depth of discharge for a low-earth-orbit regime) are shown in Fig. 5 (obtained from Johnson Controls, Inc.).[9] The process consists of a constant current charge at 6.14 A and constant current discharge at 9.19 A. During overcharge, the current efficiency drops drastically, and it reaches 2.42% at the end of charge.

The total heat-generation rate within the cell is calculated using Eq. 9 during charge and Eq. 10 during discharge with the potential and current efficiency data in Fig. 5, and the results are shown in Fig. 6 as the case I curve. The heat-generation rate of oxygen recombination with hydrogen on the platinum electrode is calculated using Eq. 8 and is shown as the case II-b curve and all heat generation except oxygen recombination is shown as the case II-a curve in Fig. 6. Heat generation by oxygen recombination is assumed to be located uniformly on the platinum electrode. All heat generation except oxygen recombination is assumed to be located uniformly on the nickel electrode. The case I curve is the sum of case II-a and II-b curves, and the volume ratio of the nickel to platinum electrode is 27:8. A finite element equation solver called PDE2D [23] was used to solve the equation. The thermal and physical property values of the cell components were obtained from the literature.[24] Figure 7a is the temperature contour plot with a heat-generation rate of 0.028 W/cm^3 only on the nickel electrode. Figure 7b is same total amount of heat generation but only on the platinum electrode. The maximum temperature of Fig. 7a is 12.8936°C and that of Fig. 7b is 12.8950°C. The temperature difference between these two is only 0.0014°C (less than 0.01%). The comparison between Fig. 7a and b shows that there is a small difference in temperature contour plots only near the right side even though the heat-generation location is different. Thus, the assumption of heat generation only on the nickel electrode is reasonable to calculate the temperature profile for the steady-state case.

Figure 8 shows the result of temperature changes during three cycles when heat generation is split between the nickel and platinum electrodes using the II-a and II-b curves in Fig. 6. The maximum temperature during overcharge is on the platinum electrode and during discharge on the nickel electrode. Figure 9 presents a comparison between the results shown in Fig. 8 and the predictions obtained from using the case I curves given in Fig. 6. The maximum temperature difference (Fig. 9c) is 0.019°C at 51 min. Thus, the assumption of heat generation only on the nickel electrode (case I) can be used to calculate the temperature profile in time-dependent cases.

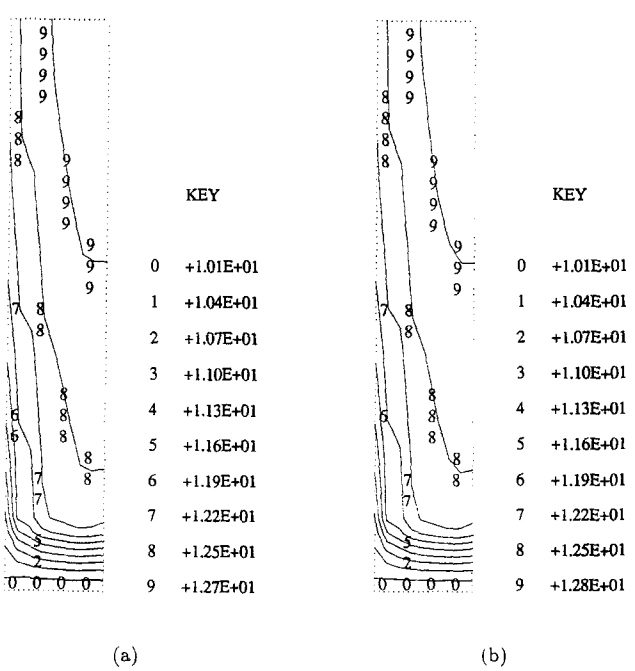

Fig. 7. Temperature contour plots at steady state with a heat-generation rate of 0.028 W/cm^3 (average value over charge and discharge cycle): (a) heat generation only on the nickel electrode, and (b) heat generation only on the platinum electrode.

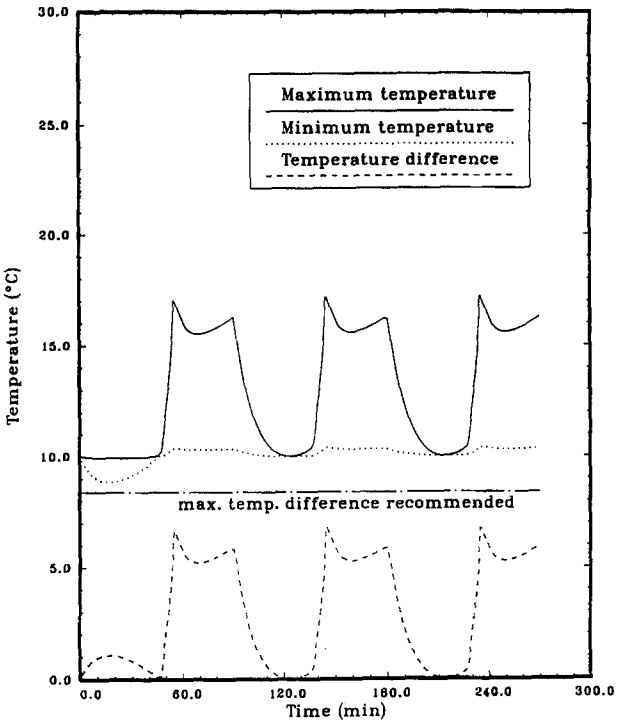

Fig. 8. Temperature change during three cycles with heat-generation rate lines II-a and II-b in Fig. 6.

Conclusion

An equation (Eq. 14) is presented that can be used to calculate the maximum allowable temperature difference inside a nickel-hydrogen battery to avoid water relocation for given temperature and electrolyte concentration ranges. A comparison between heat generation assumed to be only on the nickel electrode and heat generation on the nickel and platinum electrodes, shows that there is a very small difference in predicted temperature profiles in both the steady-state and time-dependent cases. This means that the temperature profile in the cell is not sensitive to the heat-generation location.

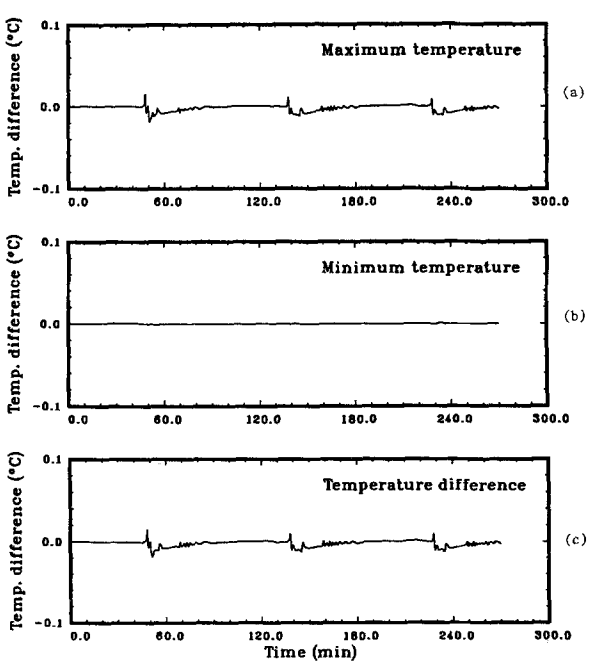

Fig. 9. The temperature differences (time-dependent cases) between using case II-a and II-b curves in Fig. 6 (heat generation is split between the nickel and platinum electrodes) and using case I curve in Fig. 6 (heat generation only on the nickel electrode); (a) maximum temperature, (b) minimum temperature, and (c) temperature difference.

Acknowledgment

The authors are grateful for the financial support of this work from the NASA Center for Space Power at Texas A&M University. Also, the authors thank J. P. Zagrodnik at Johnson Controls, Inc. for supplying useful information.

Manuscript submitted Feb. 14, 1992; revised manuscript received Oct. 8, 1993.

The University of South Carolina assisted in meeting the publication costs of this article.

LIST OF SYMBOLS

a	intersection point with $T_c = 0$ line, °C
b	slope of variable wall temperature line at one potassium hydroxide concentration
E	cell voltage, V
F	Faraday's constant, 96,487 C/eq
ΔH_a	enthalpy change for Eq. 3 during charge, 145.50 KJ · mol^{-1}
ΔH_b	enthalpy change for Eq. 6 during charge, 285.83 KJ · mol^{-1}
I	total cell current, A
M	molality of the potassium hydroxide solution, mol/1000 g of H_2O
n	number of electrons involved in an electrochemical reaction
P	cell pressure, atm
$P_{W(KOH)}$	vapor pressure over the potassium hydroxide solution, bar
Q	heat in the system, J
q_o	heat-generation rate by oxygen recombination, W
q	heat-generation rate, W
$T^\star$	temperature, K
T_c	the coldest point temperature in the nickel-hydrogen battery, °C
ΔT	the maximum allowable temperature difference in the nickel-hydrogen battery, °C
t	time, s
V	cell volume, cm^3
W	weight percent of potassium hydroxide solution
η	current efficiency during charge

REFERENCES

1. J. Giner and J. D. Dunlop, *This Journal,* **122,** 4 (1975).
2. M. A. Manzo and M. A. Hoberecht, *Intersociety Energy Conversion Engineering Conference,* **1,** 287 (1984).
3. R. L. Kerr, *ibid.,* **3,** 1521 (1986).
4. J. D. Dunlop, *NASA/GSFC Battery Workshop,* p. 389 (1982).
5. F. E. Betz, *ibid.,* p. 416 (1982).
6. K. H. Fuhr, NTIS N8811030 (1988).
7. H. H. Rogers, E. Levy, Jr., and S. J. Stadnick, APAFL-TR-77-90 (1977).
8. C. J. Johnson, *Nickel Hydroxide Electrodes,* D. A. Corrigan and A. H. Zimmerman, Editors, PV 90-4, p. 381, The Electrochemical Society Proceedings Series, Pennington, NJ (1990).
9. J. P. Zagrodnik, Personal communication.
10. D. Linden, *Handbook of Batteries and Fuel Cells,* McGraw-Hill, New York (1984).
11. P. Bro and H. Y. Kang, *This Journal,* **118,** 1430 (1971).
12. E. Washborn, *International Critical Tables of Numerical Data, Physics, Chemistry and Technology,* McGraw-Hill, New York (1928).
13. V. P. Mashovets and R. P. Matveeva, *J. Appl. Chem. USSR,* **38,** 2294 (1965).
14. V. M. Anisimov, *Russ. J. Phys. Chem.,* **47,** 601 (1973).
15. R. L. LeRoy and C. T. Bowen, *This Journal,* **127,** 1954 (1980).
16. J. Balej, *Int. J. Hydrogen Energy,* **10,** 233 (1985).
17. B. I. Tsenter and I. S. Dankova, *Sov. Electrochem.,* **14,** 1084 (1978).
18. W. R. Scott and D. W. Rusta, NASA Reference Publication 1052, NAS5-23514, p. 102 (1979).
19. W. M. Latimer, *The Oxidation States of the Elements and Their Potentials in Aqueous Solutions,* 2nd ed., Prentice-Hall, Inc., Englewood Cliffs, NJ (1952).
20. J. A. Dean, *Lange's Handbook of Chemistry,* 13th ed., McGraw-Hill, New York (1985).

21. B. I. Tsenter, A. G. Khotyaintsev, and N. N. Milyutin, *Pow. Eng., J. Acad. Sci. USSR,* **23,** 135 (1985).
22. J. S. Milton and J. C. Arnold, *Introduction to Probability and Statistics,* 2nd ed., McGraw-Hill, New York (1990).
23. PDE2D, a computer program, contact: Dr. Granville Sewell, P.O. Box 12141, El Paso, TX, Phone 915-747-6845 for additional information.
24. J. B. Kim, T. V. Nguyen, and R. E. White, *This Journal,* **139,** 2781 (1992).

Properties of Electrochemically Cation-Doped Poly(isothianaphthene)

Mitsuyoshi Onoda and Hiroshi Nakayama

Department of Electrical Engineering, Faculty of Engineering, Himeji Institute of Technology, Himeji, Hyogo 671-22, Japan

Shigenori Morita and Katsumi Yoshino

Department of Electronic Engineering, Faculty of Engineering, Osaka University, Suita, Osaka 565, Japan

ABSTRACT

The electrochemical and optical properties of poly(isothianaphthene) (PITN) during electrochemical doping have been investigated by cyclic voltammetry and optical absorption spectrum measurements. PITN can be reversibly cation- and anion-doped without decomposition of the material. This polymer, PITN, with these two reversible and stable redox states of different colors is a potential candidate for electrochromic displays. The existence of a residual charge (positive or negative) depending on the electrochemical cycle is pointed out and conditions to obtain the more or less full neutralization of this residual charge are described. Further, a reading-writing device using a residual charge which remains PITN after the dedoping has been proposed.

Since the discovery of conducting organic polymers twenty years ago, there has been much data collected to give more information on the physicochemical properties of such compounds.[1,2] That the conductivity of these materials can be controlled on doping has stimulated a wide range of studies: electrochemical, chemical, spectrochemical, etc.

Among several preparation methods for conducting polymers, electrochemical preparation is intensely interesting. For example, polythiophene (PT) films can be easily grown in their oxidized conducting form on a conductive substrate by the electrochemical polymerization of thiophene monomer. The use of PT films as active elements in electrochromic display devices has been proposed on the basis of their electro-optical properties.[3]

Transparent conducting films with various properties, such as optical transparency and high reflection in the infrared region, etc., are important in the field of optoelectronics. So far, metallic thin films and oxide semiconductors have been widely used as transparent conducting films. However, in inorganic materials such as indium tin oxide (ITO), substrates on which conducting films were formed were restricted because a very high temperature is required to produce such films. Recently, PITN [$((C_8H_4S)_x)$] was found to be transparent and colorless in the doped conducting state.[4] PITN can be prepared by the electrochemical polymerization of isothianaphthene. PITN in the undoped state has the smallest bandgap of *ca.* 1 eV in the family of conjugated polymers. On doping, PITN becomes colorless. This fact indicates that transparent conducting films can be prepared with even organic conducting polymers and low temperature processing is possible.

For practical application of conducting polymers, it is desirable that the conducting polymers can be doped by both anion and cation in a reversible manner. However, a study of cation doping is hardly ever carried out because of greater difficulties compared to anion doping. So far a restricted number of conducting polymers such as PT, poly(p-phenylene) (PPP), poly(1,4-naphthalene vinylene) (PNV), and poly(2.5-thienylene vinylene) (PTV) can be doped with cations with a high stability.[5-8] The electrochemical cycle of anion or cation doping in conducting polymers has been useful in a rechargeable battery and in electro-optic color switching devices.[9,10] It is also interesting from practical viewpoints whether cation doping is possible in PITN or not. Kobayashi *et al.* have reported that cation doping in PITN was very difficult.[4] However, we have clarified the electronic band scheme of PITN in comparison with that of PT by *in situ* optical and magnetic measurements during electrochemical anion doping, from which successful cation doping in PITN was expected.[11]

This article is concerned with the fundamental electrochemical properties of cation-doped PITN, *i.e., in situ* optical and electrochemical properties of PITN have been studied by electrochemical cyclic voltammetry and optical absorption spectroscopy measurements.

Experimental

Materials.—Isothianaphthene was prepared according to a similar procedure to that described in detail in our previous publications.[11] Tetrabutylammonium tetrafluoroborate (Bu_4NBF_4) was recrystallized three times from methanol + water (1:1) and dried 72 h, at 60°C under vacuum. Acetonitrile (AN) was dried and distilled several times in the usual manner before use.

Electrochemical polymerization and measurements.—The apparatus and procedure for electrochemical polymerization of isothianaphthene were the same as those described previously.[11] The molecular structure of PITN is shown in Fig. 1.

All the electrochemical investigations were carried out in a three-compartment cell: the anode, the cathode, and the reference electrode were in all cases separated by a glass frit. All potentials are referred to the Ag/Ag^+ system, Bu_4NBF_4 (0.2 mol/liter) in AN. The working and cathode electrodes were an indium tin oxide (ITO)-coated conducting glass substrate and a platinum grid, respectively. All the experiments were performed under argon atmosphere, using a Hokuto Denko Ltd. Model HA-303 potentiostat and a Hokuto Denko Ltd. Model HB-105 signal generator. The cyclic voltammograms were recorded on a Pantos U-335 X-Y recorder. The *in situ* optical absorption spectroscopy measurements during electrochemical doping were carried out using a Hitachi 330 spectrophotometer. For absorption